Magneto-optical properties of Rydberg excitons: Center-of-mass quantization approach

Sylwia Zielińska-Raczyńska, David Ziemkiewicz,* and Gerard Czajkowski
Institute of Mathematics and Physics, UTP University of Science and Technology, Al. Prof. S. Kaliskiego 7, 85-789 Bydgoszcz, Poland
(Received 10 October 2016; revised manuscript received 14 December 2016; published 9 February 2017)

We show how to compute the magneto-optical functions (absorption, reflection, and transmission) when Rydberg exciton polaritons appear, including the effect of the coherence between the electron-hole pair and the electromagnetic field, and the polaritonic effect. Using the real density-matrix approach the analytical expressions for magneto-optical functions are obtained and numerical calculations for Cu_2O crystal are performed. The influence of the strength of applied external magnetic field on the resonance displacement of excitonic spectra is discussed. We report a good agreement with recently published experimental data.

DOI: 10.1103/PhysRevB.95.075204

I. INTRODUCTION

The concept of excitons was formulated more than 80 years ago by Frenkel [1], who predicted their existence in molecular crystals. A few years later, Wannier [2] and de Mott [3] described these electron-hole bound states for inorganic semiconductors. In 1952 Gross and Karriiev [4] discovered such Wannier-Mott excitons experimentally in a copper oxide semiconductor. Since that time excitons have remained an important topic of experimental and theoretical research, since they play a dominant role in the optical properties of semiconductors (molecular crystals, etc.). Excitons have been studied in great detail in various types of semiconductor nanostructures and in bulk crystals. Since there is a large number of papers, monographs, and review articles devoted to excitons, we refer to only a small collection of them [5–10]. In the past decades the main effort of the researchers was focused on excitons in nanostructures [11–21], but very recently, new attention has been drawn back to the subject of excitons in bulk crystals by an experimental observation of the so-called yellow exciton series in Cu_2O up to a large principal quantum number of $n = 25$. [22] Such excitons in copper oxide, in analogy to atomic physics, have been named Rydberg excitons. By virtue of their special properties Rydberg excitons are of fascination in solid and optical physics. These objects whose size scales as the square of the Rydberg principal quantum number n are ideally suited for fundamental quantum interrogations, as well as detailed classical analysis. Several theoretical approaches to calculate optical properties of Rydberg excitons have been presented [23–35]. Recently quantum coherence of Rydberg excitons in this system has been investigated [34] which opens an avenue for their further implementation in quantum information processing.

When external constant fields (electric or/and magnetic) are applied, the Rydberg excitons, especially those with high principal number n, show effects which are not observable in exciton systems with a low number of excitonic states. This effect ranges from a large Stark shift, overlapping of states, creation of higher-order excitons (F, H, etc.) to quantum chaos and type of statistics for exciton states [31]. Although the Stark and other electro-optic effects on Rydberg excitons in Cu_2O have been measured and analyzed [24,25,32], there are only few results available regarding the magneto-optic properties of Rydberg excitons [31] where the excitonic spectra of cuprous oxide subjected to an external magnetic field up to 7 T have been measured and the complex splitting patterns of crossing and overlapping levels have been demonstrated.

Highly excited Rydberg excitons in Cu_2O crystal provide a well-accessible venue for combined theoretical and experimental studies of magnetic field effects on the systems. From a different perspective magnetic fields may offer a promising possibility for a controlled manipulation of Rydberg excitons, which would be otherwise difficult to trap by standard optical techniques, developed for ground states. Due to the fact that free-space Rydberg polaritons have recently drawn intense interest as tools for quantum information processing one can expect that Rydberg excitons in solid may become highly required object for creating high-fidelity photonic quantum materials [36]. Magnetic fields can strongly affect the Rydberg-Rydberg interactions by breaking the Zeeman degeneracy that produces Foster zeros.

In the present paper we will focus on magneto-optical properties of Rydberg excitons in Cu_2O motivated by the results presented in Ref. [31]. As in our previous papers [26,32], we will use the method based on the real density-matrix approach (RDMA). Our main purpose is to obtain the analytical expressions for the magneto-optical functions of semiconductor crystals (reflectivity, transmissivity, absorption, and bulk magnetosusceptibility), including a high number of Rydberg excitons, taking into account the effect of anisotropic dispersion and the coherence of the electron and hole with the radiation field, as well to calculate the positions of excitonic resonances in the situation when degeneracies of exciton states with different orbital and spin angular momentum are lifted by magnetic field. The present approach, owing to application of the full form of Hamiltonian for excitons in an external magnetic field, allows one to get so-called positive shifts of resonances (connected with a linear dependence on the field strength and quadratic exciton diamagnetic shifts). Due to the specific structure of Cu_2O crystal, particulary to a small radius of Wannier excitons, it is justified to assume infinite confinement potentials at the crystal surface. All these factors result in a complex pattern of spectra which, especially for higher order of excitons, becomes even more intricate for states with higher principal number n.

In a very recent paper Schweiner *et al.* [34] have pointed out that an external magnetic field influences the system, reducing

*david.ziemkiewicz@utp.edu.pl

its cubic symmetry, and leads to the complex splitting of excitonic lines in absorption spectra. They have solved numerically the Schrödinger equation and then calculated oscillator strengths including the complete valence-band structure into their considerations. The most results for Rydberg excitons was concentrated on the energy values of the excitonic states (for example, [33]). We, in turn, extend such an approach including the polariton effects. This will be done by means of the so-called center-of-mass (COM) quantization approach [37–47]. Thanks to this approach one can include into account the influence of the internal structure of the electromagnetic wave propagating in the crystal. It is important because in the experiments on the Rydberg excitons in Cu_2O [22,24,31] the crystal size in the propagation direction exceeds largely the wavelength. Finally, we will examine the influence of the effective-mass anisotropy on the magneto-optic properties.

The paper is organized as follows. In Sec. II we recall the basic equations of the RDMA and formulate the equations for the case when the constant magnetic field is applied. In Sec. III we describe an iteration procedure, which will be applied to solve a system of coupled integrodifferential equations and finally obtain the magneto-optic functions. The second iteration step, from which the magneto-optic functions, including the polariton effects, will be calculated, is given in Sec. IV. The formulas, derived in this section, are than applied in Sec. V to calculate the magneto-optic functions for a Cu_2O crystal, considered in Ref. [31]. Finally, in Sec. VI we draw conclusions of the model studied in this paper. The derivations of useful matrix elements and calculations with a lot of technical details are established in the appendixes.

II. DENSITY-MATRIX FORMULATION

Having in mind the above-mentioned experiments on Rydberg excitons, we will compute the linear response of a semiconductor slab to a plain electromagnetic wave, whose electric-field vector has a component of the form

$$E_i(z,t) = E_{\text{in}} \exp(ik_0 z - \mathrm{i}\omega t), \quad k_0 = \frac{\omega}{c}, \tag{1}$$

attaining the boundary surface of the semiconductor located at the plane $z = 0$. The second boundary is located at the plane $z = L$. In the case of the examined Cu_2O crystals the extension will be of the order 30 μm.

The electromagnetic wave is then reflected, transmitted, and partially absorbed. The wave propagating in the medium has the form of polaritons, defined as joint field-medium excitations. Polaritons are mixed modes of the electromagnetic wave and discrete excitations of the crystal (excitons). Below we assume the separation of the relative electron-hole motion with well defined quantum levels and the center-of-mass motion which interacts with the radiation field and produces the mixed modes.

The real density-matrix approach (RDMA), which we wish to apply below, is the extension to crystal states of the Bloch equations of atomic physics, and allows the calculation of transition probability amplitudes including lifetime effects. It takes into account the following contributions: (a) the electron-hole interaction, (b) the dipole interaction between the electron-hole pairs and the electromagnetic field, (c) the particle-surface interaction, (d) *effects of external fields.* We consider a semiconductor in the real-space representation, characterized by a number of valence and conduction bands. Electrons at site j in the conduction band are described by fermion operators $\hat{c}_j^{c\dagger}(\hat{c}_j^c)$ which correspond to the creation (annihilation) operators. Similarly, operators $\hat{d}_j^{v\dagger}(\hat{d}_j^v)$ are creation (annihilation) operators for holes in valence bands at site j. The physical quantities which are most relevant for the optical properties can be expressed in terms of mean values of the following pair operators:

$$\begin{aligned} &\text{excitonic transition density amplitude,} \quad Y_{12}^{\alpha b} = \langle \hat{d}_1^{\alpha}\, \hat{c}_2^{b} \rangle, \\ &\text{electron density,} \quad C_{12}^{ab} = \langle \hat{c}_1^{a\dagger} \hat{c}_2^{b} \rangle, \\ &\text{hole density,} \quad D_{12}^{\alpha\beta} = \langle \hat{d}_1^{\alpha\dagger} \hat{d}_2^{\beta} \rangle, \end{aligned} \tag{2}$$

where the indices $a,b,\ldots$ label the conduction bands, and $\alpha,\beta,\ldots$ label the valence bands. The detailed derivation, which leads to the constitutive equations for the above quantities, can be found in Refs. [7,9]. Here we restrict our consideration to the lowest order related to linear optics, by setting the matrices $C = D = 0$, and use only the excitonic amplitudes $Y^{\nu}(\mathbf{r}_e,\mathbf{r}_h)$ of the electron-hole pair of coordinates $\mathbf{r}_h$ (hole) and $\mathbf{r}_e$ (electron). In the case of Cu_2O, ν means $P,F,H,\ldots$ excitons. The constitutive equations have the form (see also [26,32])

$$\begin{aligned} &\dot{Y}(\mathbf{R},\mathbf{r}) + (i/\hbar) H_{\text{eh}} Y(\mathbf{R},\mathbf{r}) + (1/\hbar)\Gamma Y(\mathbf{R},\mathbf{r}) \\ &\quad = (i/\hbar)\mathbf{M}(\mathbf{r})\mathbf{E}(\mathbf{R}), \end{aligned} \tag{3}$$

where $\mathbf{R}$ is just the excitonic center-of-mass coordinate, $\mathbf{r} = \mathbf{r}_e - \mathbf{r}_h$ is the relative coordinate, $\mathbf{M}(\mathbf{r})$ is the smeared-out transition dipole density, $\mathbf{E}(\mathbf{R})$ is the electric-field vector of the wave propagating in the crystal, and operator Γ stands for the dissipation processes; we assume that it is nonnegative and commutes with H_{eh}. The smeared-out transition dipole density $\mathbf{M}(\mathbf{r})$ is related to the bilocality of the amplitude Y and describes the quantum coherence between the macroscopic electromagnetic field and the interband transitions. The two-band Hamiltonian H_{eh} includes the electron- and hole-kinetic-energy terms, the electron-hole interaction potential, and the confinement potentials. When constant fields, magnetic and electric, are applied, the Hamiltonian has the form

$$\begin{aligned} H = {} & E_g + \frac{1}{2m_e}\left(\mathbf{p}_e - e\frac{\mathbf{r}_e \times \mathbf{B}}{2}\right)^2 + \frac{1}{2m_{hz}}\left(\mathbf{p}_h + e\frac{\mathbf{r}_h \times \mathbf{B}}{2}\right)_z^2 \\ & + \frac{1}{2m_{h\parallel}}\left(\mathbf{p}_h + e\frac{\mathbf{r}_h \times \mathbf{B}}{2}\right)_{\parallel}^2 + e\mathbf{F}\cdot(\mathbf{r}_e - \mathbf{r}_h) \\ & + V_{\text{conf}}(\mathbf{r}_e,\mathbf{r}_h) - \frac{e^2}{4\pi\epsilon_0\epsilon_b|\mathbf{r}_e - \mathbf{r}_h|}. \end{aligned} \tag{4}$$

$\mathbf{B}$ is the magnetic field vector, $\mathbf{F}$ is the electric-field vector, V_{conf} are the surface potentials for electrons and holes, $m_{hz}, m_{h\parallel}$ are the components of the hole effective-mass tensor, and the electron mass is assumed to be isotropic. Separating the exciton center-of-mass and relative motion, and considering the case when $\mathbf{B} \parallel z$, $\mathbf{F} = 0$, we transform the Hamiltonian (4) into the

form

$$H = H_0 + \frac{P_z^2}{2M_z} + \frac{\mathbf{P}_\parallel^2}{2M_\parallel} + \frac{1}{8}\mu_\parallel \omega_c^2 \rho^2 + \frac{e}{2\mu_\parallel'} B\mathcal{L}_z - \frac{e}{M_\parallel}\mathbf{P}_\parallel \cdot (\mathbf{r}_\parallel \times \mathbf{B}) + V_{\rm conf}(\mathbf{R},\mathbf{r}), \quad (5)$$

where $\omega_c = eB/\mu_\parallel$ is the cyclotron frequency, the reduced mass $\mu_\parallel'$ is defined as

$$\frac{1}{\mu_\parallel'} = \frac{1}{m_e} - \frac{1}{m_{h\parallel}}, \quad (6)$$

and H_0 is the two-band Hamiltonian for the relative electron-hole motion,

$$H_0 = -\frac{\hbar^2}{2\mu_\parallel}\nabla \underline{\underline{\mu}} \nabla - \frac{e^2}{4\pi\epsilon_0\epsilon_b|\mathbf{r}_e - \mathbf{r}_h|}, \quad (7)$$

as used in the papers [26,32], with $\underline{\underline{\mu}}$ being the exciton reduced mass tensor. The operator $\mathcal{L}_z$ is the z component of the angular momentum operator. We must solve the constitutive equations with the above Hamiltonian to obtain the polarization and finally the polariton modes.

The coherent amplitudes Y define the excitonic counterpart of the polarization,

$$\mathbf{P}_{\rm exc}(\mathbf{R}) = 2\int d^3r \mathbf{M}^*(\mathbf{r}) Y(\mathbf{R},\mathbf{r}), \quad (8)$$

which is that used in the Maxwell field equation,

$$c^2\nabla_R^2\mathbf{E} - \underline{\underline{\epsilon}}_b\ddot{\mathbf{E}}(\mathbf{R}) = \frac{1}{\epsilon_0}\ddot{\mathbf{P}}_{\rm exc}(\mathbf{R}), \quad (9)$$

with the use of the bulk dielectric tensor $\underline{\underline{\epsilon}}_b$ and the vacuum dielectric constant ϵ_0. In the present paper we solve Eqs. (3)–(9) with the aim to compute the magneto-optical functions (reflectivity, transmission, and absorption) for the case of Cu_2O.

In semiconductors like, e.g., GaAs, when only a few lowest excitonic states are excited, it is possible to solve the polariton dispersion relation and to determine the amplitudes of the polariton waves. Analogous methods cannot be applied in the case of Rydberg excitons, whereas, for example, in Cu_2O, even 25 excitonic states are observed. There is a question of what approach is appropriate for such a case. One of the possibilities is to use the above-mentioned exciton center-of-mass quantization. In this approach it is assumed that no electron or hole separately is confined, but their center-of-mass is confined within the crystal [37–47]. This approach is justified for small-radius Wannier excitons, as is the case of Cu_2O (about 1 nm), and certainly not appropriate for semiconductors with large-radius excitons, like GaAs (about 15 nm). In the COM approach mostly infinite confinement potentials at the crystal surfaces $z = 0, L$ are assumed, therefore the eigenfunctions and eigenvalues of the COM motion have the form

$$w_N(Z) = \sqrt{\frac{2}{L^*}}\sin\left(\frac{N\pi}{L^*}Z\right), \quad W_N = \frac{\hbar^2}{2M_z}\frac{N^2\pi^2}{L^{*2}} = N^2 S,$$
$$S = \frac{\mu_\parallel}{M_z}\left(\frac{\pi a^*}{L^*}\right)^2 R^*, \quad (10)$$

where M_z is the total excitonic mass in the z direction, a^* is the excitonic radius, R^* is the excitonic Rydberg, and L^* is the effective crystal size in the z direction. When assuming the existence of exciton free surface layers with the thickness $L_{\rm ef}$, we are left with the bulk region of the dimension $L^* = L - 2L_{\rm ef}$ where the exciton polaritons are formed. This dimension is sometimes called the effective crystal size. Since, in the case of Cu_2O, the $L_{\rm ef}$, being comparable with the excitonic Bohr radius, are very small, we assume $L* = L$ (L being the crystal size in the z direction).

Having the confinement functions, we look for a solution of the form

$$Y(Z,\mathbf{r}) = \sum_{N\ell m} c_{N\ell m} R_{n\ell m}(r) Y_{\ell m}(\theta,\phi) w_N(Z), \quad (11)$$

where $R_{n\ell m}$ are the radial functions of an anisotropic Schrödinger equation [32],

$$R_{n\ell m}(r) = \left(\frac{2\eta_{\ell m}}{na^*}\right)^{3/2}\frac{1}{(2\ell+1)!}\sqrt{\frac{(n+\ell)!}{2n(n-\ell-1)!}} \times \left(\frac{2\eta_{\ell m} r}{na^*}\right)^\ell e^{-\eta_{\ell m} r/na^*} \times M\left(-n+\ell+1, 2\ell+2, \frac{2\eta_{\ell m} r}{na^*}\right),$$
$$\eta_{\ell m} = \int d\Omega \frac{|Y_{\ell m}|^2}{\sin^2\theta + (\mu_\parallel/\mu_z)\cos^2\theta}, \quad (12)$$

and $E_{n\ell m}$ are the corresponding eigenvalues,

$$E_{n\ell m} = -\frac{\eta_{\ell m}^2}{n^2}R^*, \quad (13)$$

$M(a,b,z)$ being the confluent hypergeometric function in the notation of [48].

III. ITERATION PROCEDURE

The electric field $E(Z)$ of the wave propagating in the crystal, acting as a source in Eq. (3), must satisfy the Maxwell equation (9) which, for the wave propagating in the Z direction and with the harmonic time dependence fulfills the propagation equation

$$\frac{d^2E}{dZ^2} + k_b^2 E(Z) = -\frac{\omega^2}{c^2\epsilon_0}P_{\rm exc}(Z), \quad k_b = \sqrt{\epsilon_b}\frac{\omega}{c}, \quad (14)$$

and $P_{\rm exc}(Z)$ is the Z- dependent excitonic part of the crystal polarization (8). The function $Y(Z,\mathbf{r})$, with regard to (3) and (11), and for the Faraday configuration, satisfies the equation

$$\sum_{N\ell m}\left(E_g - \hbar\omega + W_N + E_{n\ell m} + m\frac{\mu_\parallel}{\mu_\parallel'}\gamma R^* - i\Gamma + \frac{R^*}{4a^{*2}}\gamma^2 r^2\sin^2\theta\right)c_{N\ell m}R_{n\ell}(r)Y_{\ell m}(\theta,\phi)w_N(Z) = \mathbf{M}(\mathbf{r})\mathbf{E}(Z), \quad (15)$$

where $\gamma = \hbar\omega_c/2R^*$ is the dimensionless strength of the magnetic field. Even under applying the COM quantization, we are left with a system of two coupled integrodifferential equations for the functions Y and E. Having the field $E(Z)$ we

can determine the optical functions, reflectivity, transmissivity, and absorption, by the relations

$$R = \left|\frac{E(0)}{E_{\rm in}} - 1\right|^2, \quad T = \left|\frac{E(L^*)}{E_{\rm in}}\right|^2, \quad A = 1 - R - T, \tag{16}$$

where $E_{\rm in}$ is the amplitude of the normally incident wave. The solution of Eqs. (14)–(16), which enables one to get the electric field and the optical functions, can be obtained by several methods. The specific properties of Rydberg excitons in Cu_2 make the calculations more difficult than in other semiconductors with Wannier-Mott excitons. In GaAs only the lowest exciton states contribute, which means that only few polariton waves should be taken into account, and an approximation, giving the amplitudes of the polariton waves and thus the electric field in the medium, as described in Ref. [49], can be used. In quantum dots, where, in the strong confinement limit the separation of the relative and COM motion cannot be made, one can try the direct numerical solution of the relevant Schrödinger equation, giving the eigenfunctions and eigenvalues, which, in turn, are used to solve the constitutive equation and the optical properties (see, for example, [50,51] and references therein). Both methods cannot be applied for the considered case of Rydberg excitons. When taking into account, for example, $n = 25$ excitonic states, we deal with at least the same number of polariton waves (or even twice when considering the waves in both directions) and a method to calculate their amplitudes is, to our knowledge, not known. When regarding the sample dimension of 30 μm, i.e., thousands of the excitonic Bohr radius, the direct numerical calculation exceeds the possibility of computers. This is the motivation to apply the COM approximation, connected with certain iteration procedure. The first step of this procedure is the solution of the system of equations (15), where on the right-hand side we put instead of the full solution $E(Z)$, its (known) homogeneous part $E_{\rm hom}$, satisfying the equation

$$\frac{d^2E}{dZ^2} + k_b^2 E(Z) = 0, \tag{17}$$

and the appropriate boundary conditions. It has the form

$$\begin{aligned} E_{\rm hom}(Z) &= E_{\rm in}\frac{2k_0 f(L-Z)}{(k_b+k_0)W}, \\ f(z) &= e^{-ik_bZ} + \frac{k_b-k_0}{k_b+k_0}e^{ik_bZ}, \\ W &= e^{-ik_bL} - \left(\frac{k_b-k_0}{k_b+k_0}\right)^2 e^{ik_bL}. \end{aligned} \tag{18}$$

Inserting the above expressions into the right-hand side of Eqs. (15), the following set of equations will be obtained, from which the coefficients $c_{N\ell m}$ can be determined from

$$\begin{aligned} &\sum_{N\ell m}\left(W_{N\ell m} + \frac{R^*}{4a^{*2}}\gamma^2 r^2\sin^2\theta\right) \\ &\quad\times c_{N\ell m}R_{n\ell m}(r)Y_{\ell m}(\theta,\phi)w_N(Z) \\ &\quad= \mathbf{M}(\mathbf{r})\mathbf{E}_{\rm hom}(Z), \\ &W_{N\ell m} = E_g - \hbar\omega + W_N + E_{n\ell m} + m\frac{\mu_\parallel}{\mu'_\parallel}\gamma R^* - i\Gamma. \end{aligned} \tag{19}$$

The expression for the dipole density, which should be used in (15), has the following form: for P excitons, $\ell = 1$ [26],

$$\begin{aligned} \mathbf{M}^{(1)}(\mathbf{r}) &= \mathbf{e}_r\, M_{10}\frac{r+r_0}{2r^2r_0^2}e^{-r/r_0} = \mathbf{e}_r M(r) \\ &= \mathbf{i}M_{10}\frac{r+r_0}{4ir^2r_0^2}\sqrt{\frac{8\pi}{3}}(Y_{1,-1} - Y_{1,1})e^{-r/r_0} \\ &\quad + \mathbf{j}M_{10}\frac{r+r_0}{4r^2r_0^2}\sqrt{\frac{8\pi}{3}}(Y_{1,-1} + Y_{1,1})e^{-r/r_0} \\ &\quad + \mathbf{k}M_{10}\frac{r+r_0}{2r^2r_0^2}\sqrt{\frac{4\pi}{3}}Y_{10}e^{-r/r_0}, \end{aligned} \tag{20}$$

and for F excitons, $\ell = 3$, in normalized (with respect to r) form,

$$\begin{aligned} &\mathbf{M}^{(3)}(\mathbf{r}) \\ &= \mathbf{i}M_{10}\frac{1}{r_0r^2}\left[\sqrt{\frac{3\pi}{7}}(Y_{31}-Y_{3-1}) - \sqrt{\frac{5\pi}{7}}(Y_{33} - Y_{3-3})\right]e^{-r/r_0} \\ &\quad + \mathbf{j}\frac{M_{10}}{r^2r_0}\left\{-\left[\sqrt{\frac{3\pi}{7}}(Y_{31} + Y_{3-1}) - \sqrt{\frac{5\pi}{7}}(Y_{33}+Y_{3-3})\right]\right\}e^{-r/r_0} \\ &\quad + \mathbf{k}\frac{M_{10}}{r^2r_0}\left(12\sqrt{\frac{\pi}{7}}Y_{30}e^{-r/r_0}\right). \end{aligned} \tag{21}$$

Having in mind the experiments by Aßmann *et al.* [31], we consider the field $\mathbf{B}$ as perpendicular to the crystal surface ($\parallel z$), and the wave propagating in the z direction and characterized by the electric field $\mathbf{E}$. The wave is assumed linearly polarized, $\mathbf{E} = (E_x,0,0)$, with the component $E_x = E_{\rm hom}(Z)$. Thus we take the x components of the densities $\mathbf{M}$ defined in (20) and (21),

$$M_x^{(1)}(\mathbf{r}) = M_{10}\frac{r+r_0}{4ir^2r_0^2}\sqrt{\frac{8\pi}{3}}(Y_{1-1} - Y_{11})e^{-r/r_0}, \tag{22}$$

$$\begin{aligned} M_x^{(3)}(\mathbf{r}) &= M_{10}\frac{1}{r_0r^2}\left[\sqrt{\frac{3\pi}{7}}(Y_{31} - Y_{3-1})\right. \\ &\quad \left. - \sqrt{\frac{5\pi}{7}}(Y_{33} - Y_{3-3})\right]e^{-r/r_0}, \end{aligned} \tag{23}$$

with the coherence radius r_0 [7,26,49]

$$r_0^{-1} = \sqrt{\frac{2\mu_\parallel}{\hbar^2}E_g}. \tag{24}$$

The above expression gives the coherence radius in terms of effective band parameters, but we find it convenient to treat the coherence radii as free parameters which can be determined by fitting experimental spectra. Mostly one takes it as a fraction of the respective excitonic Bohr radius. Using the above formulas, together with the expression (18) for homogeneous field $E_{\rm hom}$, we obtain, in the first step of iteration, a system of equations

$$\begin{aligned} &\sum_{n\ell m}\left[E_g - \hbar\omega + W_N + E_{n\ell m} + m\frac{\mu_\parallel}{\mu'_\parallel}\gamma R^* - i\Gamma\right. \\ &\quad \left. + \frac{R^*}{4a^{*2}}\gamma^2r^2\sin^2\theta\right]c_{N\ell m}R_{n\ell m}(r)Y_{\ell m}(\theta,\phi)w_N(Z) \\ &\quad = M_xE(Z). \end{aligned} \tag{25}$$

By appropriate integration and making use of the orthonormality of the eigenfunctions, the equations for the expansion coefficients get the form

$$
\begin{aligned}
&W_{Nn\ell m}c_{Nn\ell m} + V^{(n)}_{\ell\ell m}c_{Nn\ell m} + V^{(n)}_{\ell\ell+2m}c_{Nn\ell+2m} + V^{(n)}_{\ell\ell-2m}c_{Nn\ell-2m} = \langle w_N|E_x\rangle\langle R_{n\ell_1m_1}Y_{\ell m}|M_x\rangle,\\
&V^{(n)}_{\ell\ell m} = \frac{R^*}{4}\gamma^2\frac{(\ell^2+\ell+m^2-1)}{(2\ell-1)(2\ell+3)}\left(\frac{n}{\eta_{\ell m}}\right)^2[5n^2+1-3\ell(\ell+1)],\\
&V^{(n)}_{\ell\ell+2m} = -\frac{R^*}{4}\gamma^2\sqrt{\frac{(\ell+2-m)(\ell+1-m)(\ell+m+1)(\ell+m+2)}{(2\ell+1)(2\ell+3)^2(2\ell+5)}}\int_0^\infty \mathrm{d}\rho\rho^4\, R_{n\ell}R_{n\ell+2},\\
&V^{(n)}_{\ell\ell-2m} = -\frac{R^*}{4}\gamma^2\sqrt{\frac{(\ell-m)(\ell-m-1)(\ell+m)(\ell+m-1)}{(2\ell-3)(2\ell-1)^2(2\ell+1)}}\int_0^\infty \mathrm{d}\rho\rho^4\, R_{n\ell m}R_{n\ell-2m},
\end{aligned}
\tag{26}
$$

where we used the notation

$$
V^{(nn_1)}_{\ell\ell_1mm_1} = \frac{R^*}{4a^{*2}}\gamma^2\langle R_{n_1\ell_1m_1}|r^2|R_{n\ell m}\rangle\langle Y_{\ell_1m_1}|\sin^2\theta|Y_{\ell m}\rangle. \tag{27}
$$

As in the case of previously discussed electro-optic properties [32], we take into account only the states $n = n_1$. This assumption is justified by the fact that the diamagnetic shift, related to these matrix elements, is much smaller than the Zeeman splitting.

The effect of overlapping of different states is included in the resonant denominators. The detailed form for the coefficients $c_{Nn\ell m}$, $\langle R_{n_1\ell_1m_1}Y_{\ell_1m_1}|M_x\rangle$, $\langle E_x|w_N\rangle$ and the derivation of the matrix elements $V^{(n)}_{\ell\ell m}$ are given in Appendixes A and B. Equations (26) are the basic equations in the present paper, which will be used in the numerical calculations of the optical functions.

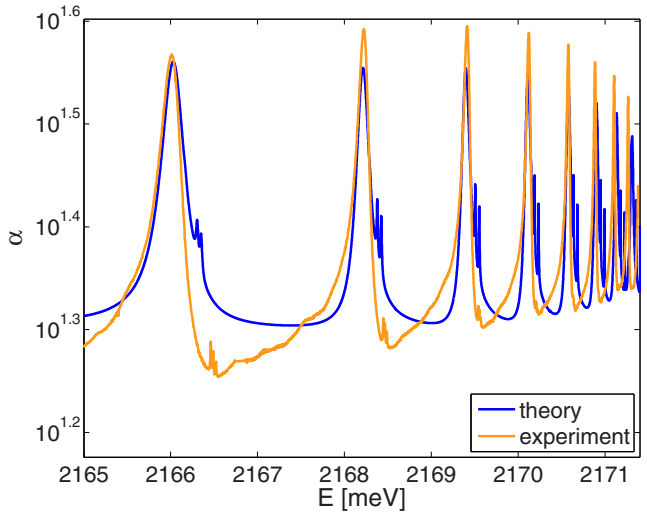

FIG. 1. The absorption A of Cu_2O crystal of thickness 30 μm and for $B = 0$, calculated from Eq. (16). A comparison between the theoretical results from Ref. [26] (blue curve), and experiments [56] (orange curve).

IV. SECOND ITERATION STEP—MAGNETOOPTIC FUNCTIONS

In the first iteration step we have computed the coefficients $c_{Nn\ell m}$. Having them, we determine the amplitude $Y(Z,\mathbf{r})$ from Eq. (11) and the excitonic polarization from Eq. (8), obtaining

$$
\begin{aligned}
P_{\mathrm{exc}}(Z) &= 2\int M^*(\mathbf{r})Y(Z,\mathbf{r})d^3r\\
&= 2\int M^*(\mathbf{r})\sum_{Nn\ell m} c_{Nn\ell m}R_{n\ell m}Y_{\ell m}w_N(Z)d^3r\\
&= \sum_N P_N w_N(Z),\\
P_N &= 2\sum_{n\ell m} c_{Nn\ell m}\langle M^*|R_{n\ell m}Y_{\ell m}\rangle\\
&= \epsilon_0\epsilon_b\Delta^{(P)}_{LT}\langle w_N|E_{\mathrm{hom}}(Z)\rangle\sum_{n\ell m}\chi_{Nn\ell m}\\
&= \epsilon_0\epsilon_b\Delta^{(P)}_{LT}I_N E_{\mathrm{hom}}(0)\sum_{n\ell m}\chi_{Nn\ell m},
\end{aligned}
\tag{28}
$$

where I_N are defined in Eq. (D6), and $\chi_{Nn\ell m}$ in Eqs. (F3) and (F4). The so-obtained polarization will be used as a source in the Maxwell equation (14). It is known that the solution of

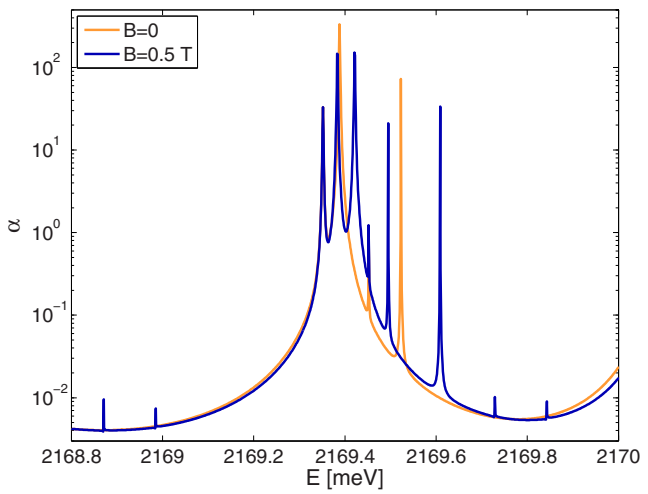

FIG. 2. Changes in absorption spectrum due to the applied magnetic field for $n = 4$ exciton.

a nonhomogeneous differential equation is composed of two parts, which are the solution of a homogeneous equation and of a nonhomogeneous one,

$$E(Z) = E_{\mathrm{hom}}(Z) + E_{\mathrm{nhom}}(Z), \tag{29}$$

where the homogeneous part satisfies Eq. (17). The nonhomogeneous part will be obtained by means of the appropriate Green function, satisfying the equation

$$\frac{\mathrm{d}^2}{\mathrm{d}Z^2} G^E(Z,Z') + k_b^2 G^E(Z,Z') = -\delta(Z - Z'), \tag{30}$$

and having the form (see, e.g., [9])

$$G^E(Z,Z') = \frac{i}{2k_b W}\left(e^{-ik_b Z^<} + \frac{k_b - k_0}{k_b + k_0} e^{ik_b Z^<}\right) \times \left(\frac{k_b - k_0}{k_b + k_0} e^{ik_b L - ik_b Z^>} + e^{-ik_b L + ik_b Z^>}\right), \tag{31}$$

where $Z^< = \min(Z,Z'), Z^> = \max(Z,Z')$. Using the above Green's function we obtain the nonhomogeneous part in the

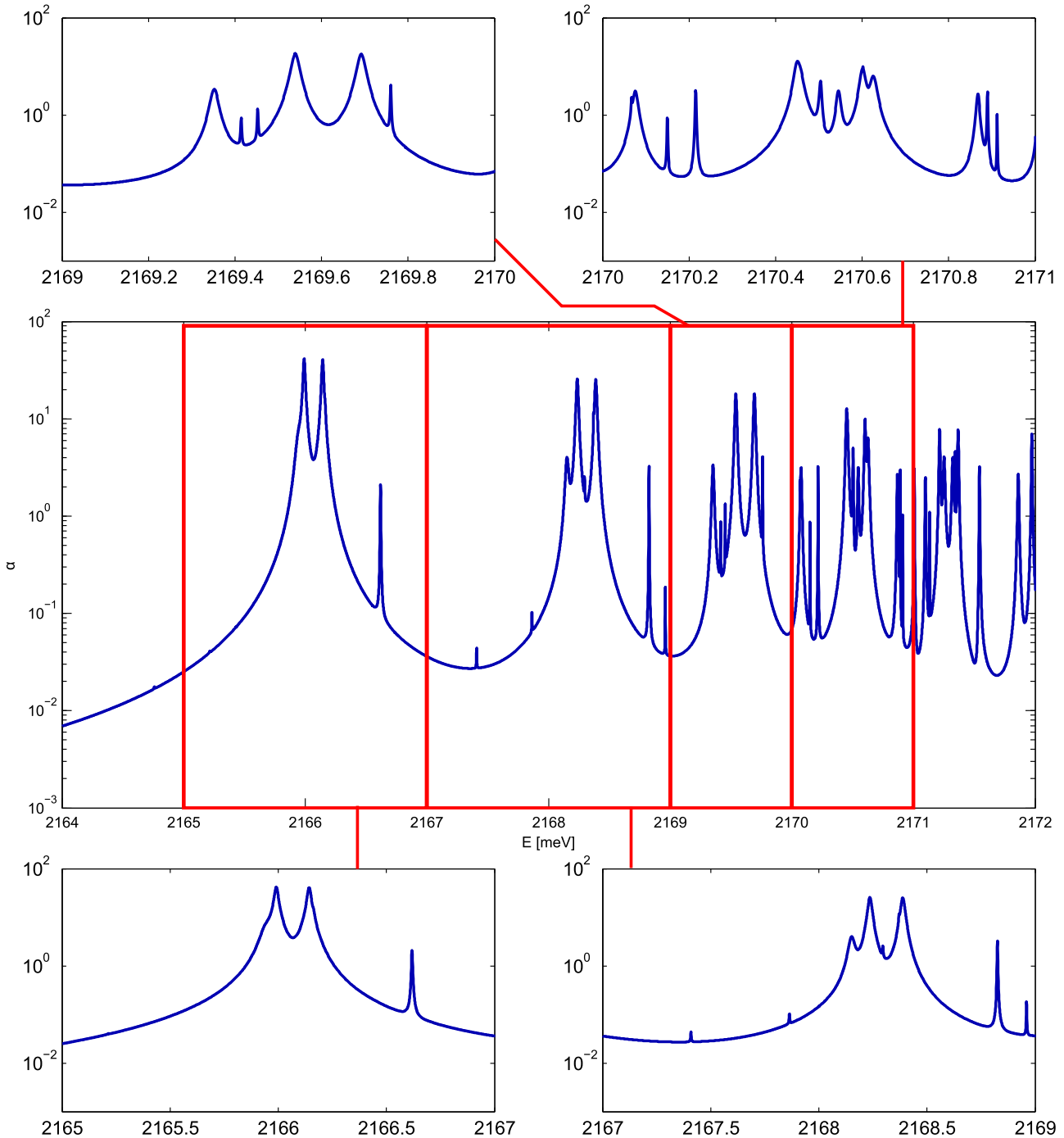

FIG. 3. The bulk magnetoabsorption of Cu_2O crystal calculated from the imaginary part of the bulk susceptibility (37) for $B = 2$ T. Insets show the detailed spectra around the excitonic lines corresponding to $n = 4, 5, 6, 7$.

form

$$E_{\rm nhom}(Z) = \frac{k_0^2}{\epsilon_0}\int_0^L G^E(Z,Z')P_{\rm exc}(Z')\mathrm{d}Z'. \quad (32)$$

Equations (29), (31), and (32) give the total electric field of the wave propagating in the crystal, from which the reflectivity R and transmissivity T are obtained. They have the form

$$R = \left|\frac{E(0)}{E_{\rm in}} - 1\right|^2 = R_{\rm FP}\left|1 + \mathrm{i}\left(\frac{k_b L}{2}\right)\frac{(1-r_\infty^2)(1-r_\infty e^{\mathrm{i}\Theta})^2(1-r_\infty^2 e^{\mathrm{i}\Theta})}{r_\infty(1-e^{\mathrm{i}\Theta})} \times \sum_N\left(\frac{I_N^2}{L}\right)\sum_{n\ell m}\Delta_{LT}^{(P)}\chi_{Nn\ell m}\right|^2, \quad (33)$$

$$T = \left|\frac{E(L)}{E_{\rm in}}\right|^2 = T_{\rm FP}\left|1 + \mathrm{i}\left(\frac{E}{2E_L}\right)\frac{(1-r_\infty e^{\mathrm{i}\Theta})}{(1-r_\infty^2 e^{\mathrm{i}\Theta})}\sum_N\left(\frac{I_N^2}{L}\right) \times \sum_{n\ell m}\Delta_{LT}^{(P)}\chi_{Nn\ell m}\right|^2, \quad (34)$$

where $\Theta = 2k_b L$, r_∞ is defined by

$$r_\infty = \frac{k_0 - k_b}{k_0 + k_b}, \quad (35)$$

I_n^2/L are given in Eq. (D7), and $R_{\rm FP}, T_{\rm FP}$ are the well-known formulas for the Fabry-Perot normal incidence reflectivity and transmissivity of a lossless dielectric slab of thickness L (see, e.g., [52]),

$$R_{\rm FP} = \frac{F\sin^2(\Theta/2)}{1+F\sin^2(\Theta/2)}, \quad T_{\rm FP} = \frac{1}{1+F\sin^2(\Theta/2)}, \quad F = \frac{4r_\infty^2}{(1-r_\infty^2)^2}. \quad (36)$$

The derivation of formulas (33) and (34) is given in Appendix E.

V. RESULTS

We have performed numerical calculations of magneto-optical functions (absorption, reflectivity, and transmissivity) for the Cu_2O crystal having in mind the experiments by Aßmann *et al.* [31]. Considering the specific properties of Cu_2O and the crystal dimension, which is large compared to the exciton Bohr radius, we observe that the COM quantized energies W_N (10) are small compared to the remaining components of the excitonic energies $W_{Nn\ell m}$ (19). Therefore, in the first approximation, we can neglect them in the formulas defining the coefficients $c_{Nn\ell m}$ (Appendix A) and in expressions $\chi_{Nn\ell m}$ (F3) and (F4), and calculate the bulk magnetosusceptibility:

$$\chi(\omega) = \epsilon_b\Delta_{LT}^{(P)}[\chi_{N211} + \chi_{N21-1} + \chi_{N311} + \chi_{N31-1} + \chi_{Nn3\pm3} + \tilde{\chi}_{Nn1\pm1} + \tilde{\chi}_{Nn3\pm1}\ldots]. \quad (37)$$

Using the formula $\alpha = (\omega/c)\mathrm{Im}\sqrt{\epsilon_b + \chi}$ we have calculated the magnetoabsorption, taking into account the lowest $n = 2$–10 excitonic states. The parameters we used are the energies $E_{n\ell m}$, the gap energy E_g, the LT energy $\Delta_{LT}^{(P)}$, and the dissipation parameter Γ. We have used the electron and hole effective masses: $m_e = 1.01$, $m_{h\parallel} = 0.5587$, $\mu_\parallel = 0.3597$, $\mu_z = 0.672$ (the masses in free electron mass) m_0, and from them calculated the reduced mass $\mu'_\parallel = -1.25$, which gives $\mu_\parallel/\mu'_\parallel \approx -0.2876$. By the relation

$$R^* = \frac{\mu_\parallel}{m_0}\frac{13\,600}{\epsilon_b^2}, \quad (38)$$

using the Cu_2O dielectric constant $\epsilon_b = 7.5$, we determined the value $R^* = 86.970$ meV. Since the longitudinal-transverse splitting energy Δ_{LT} splitting for P excitons is not known, we have established a relation between the known Δ_{LT} for S excitons and the quantity $\Delta_{LT}^{(P)}$ for P excitons. First, using the bulk dispersion

$$\frac{c^2k^2}{\omega^2} = \epsilon_b + \frac{2}{\epsilon_0}\int d^3r M^* Y, \quad (39)$$

for $k = 0, n = 2$, we establish the relation between the splitting and the dipole matrix element

$$\epsilon_b\Delta_{LT}^{(P)} = \frac{2}{\epsilon_0}|I_1 + I_2|^2\left[\frac{1}{W_{111}} + \frac{1}{W_{11-1}}\right]\Big|_{B=0}, \quad |M_{10}|^2 = \frac{4\epsilon_0\epsilon_b a^{*3}\Delta_{LT}^{(P)}}{\pi(r_0/a^*)^2\eta_{11}^5}, \quad (40)$$

where I_1, I_2 are defined in Eqs. (B3) and (B4). Using an analogous expression for for S excitons [53],

$$|M_{10}|^2 = \frac{\pi\epsilon_0\epsilon_b a^{*3}\Delta_{LT}^{(S)}}{\eta_{00}^3},$$

one can determine $\Delta_{LT}^{(P)}$ as a function of $\Delta_{LT}^{(S)}$,

$$\Delta_{LT}^{(P)} = \frac{\pi^2}{4}\left(\frac{r_0}{a^*}\right)^2\frac{\eta_{11}^5}{\eta_{00}^3}\Delta_{LT}^{(S)}. \quad (41)$$

The energies $W_{Nn\ell m}$ were obtained from relations (13) and (19) (without W_N) with the effective Rydberg energy R^*. We have used the values $E_g = 2172$ meV [52,54], $R^* = 86.970$ meV, $\Delta_{LT}^{(S)} = 10\ \mu$eV [52,55], and $\mu_\parallel/\mu_z = 0.5351$. We have restricted the upper limit of energy for our numerical illustrations

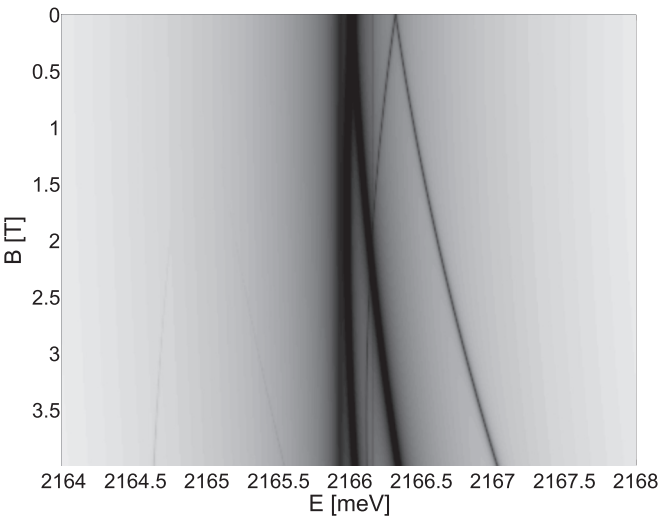

FIG. 4. Absorption spectrum in the energetic region of $n = 4$ excitonic state as a function of the applied magnetic field strength.

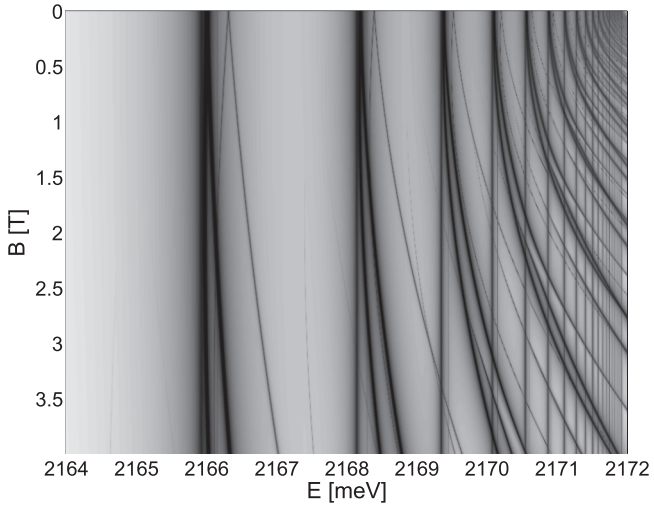

FIG. 5. The same as in Fig. 4, in the energetic region of $n = 4$–25 excitonic states.

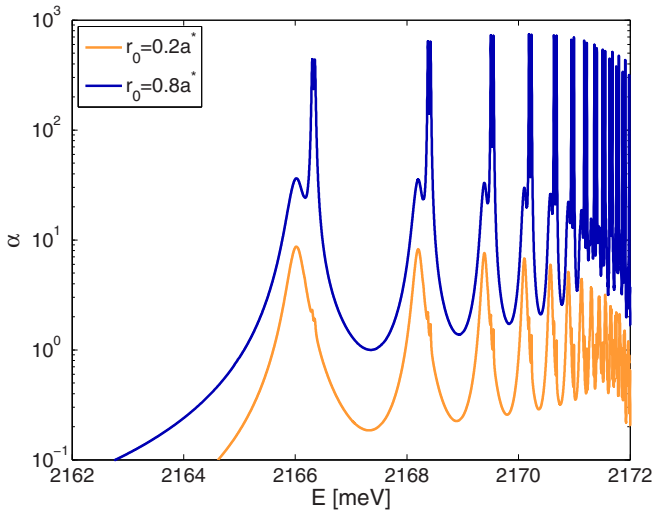

FIG. 7. The influence of the choice of the coherence radius r_0 on the magnetoabsorption spectra of Cu_2O crystal.

to 2172 meV, which determines the band gap; above this energy one could take into account effects which follow from interaction with the continuous spectrum. The choice of the set of parameters is confirmed by the excellent agreement of our theoretical absorption spectra with experimental data for the case $B = 0$ [56]; see Fig. 1. Fitting the experimental data we have determined the damping parameters Γ_n [the eigenvalues of the damping operator Γ; see Eq. (3)], which were then used in further calculations. The results for the absorption, which seem the most important, are reported in Figs. 2–7. In Fig. 2 we observe how the applied magnetic field changes the spectra. The positions of absorption maxima are changed due to the diamagnetic shift, and the Zeeman splitting occurs. The same effects, for a larger number of excitonic states and stronger field, are displayed in Fig. 3. For the principal quantum number $n \geqslant 4$ the effects due to both P and F excitons, for example, the overlapping of states, are observed. This is shown in Fig. 4 for the $n = 4$ exciton state, where the dependence of the absorption on the applied field strength is shown. The Zeeman splitting is clearly visible and the lines are shifted towards higher energy with increasing field strength. Moreover, some absorption lines become visible only for sufficiently strong magnetic field. Our calculation scheme can be extended to higher principal quantum number; the absorption spectrum for $n = 4$–25 excitonic states is shown in Fig. 5. In Fig. 6 we show that our method allows us to identify the excitonic states. In the RDMA approach we consider the role of the coherence of the radiation field with excitons, which enters *via* the smeared dipole density $\mathbf{M}(\mathbf{r})$ and its parameters $\mathbf{M}_0, r_0$. The influence of the coherence radius r_0 is illustrated in Fig. 7. One can observe that an increase of r_0 causes an increase of absorption, which is due to the related increase of the longitudinal-transverse splitting and oscillator strength;

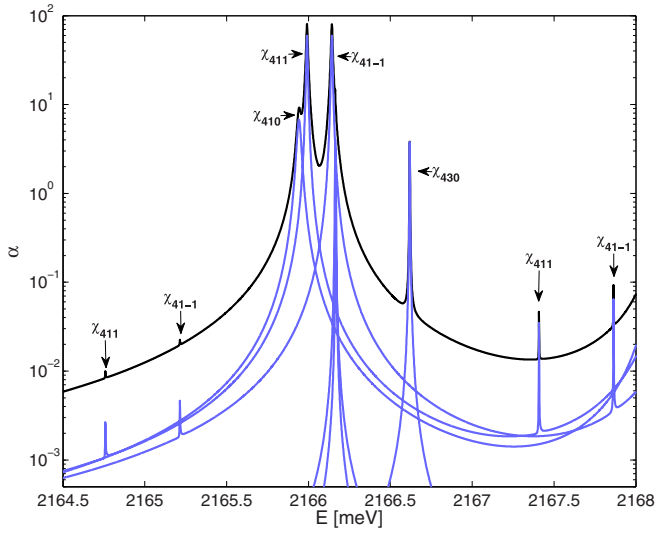

FIG. 6. The bulk magnetoabsorption of Cu_2O crystal, individual excitonic resonances are identified.

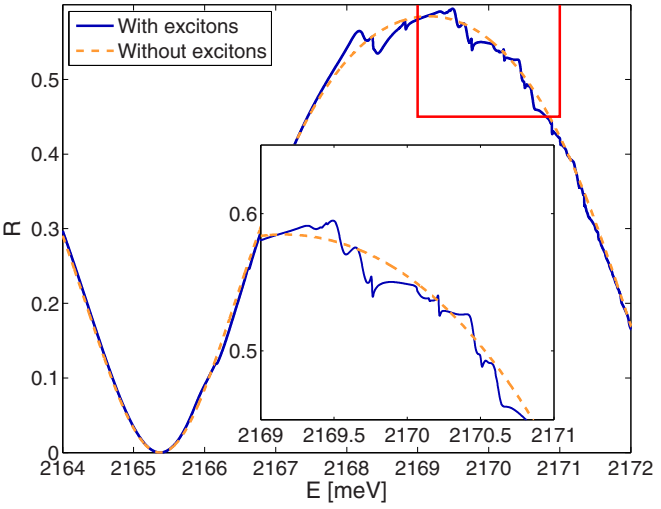

FIG. 8. The magnetoreflection coefficient of Cu_2O crystal of thickness 30 μm, when the magnetic field 2 T is applied. The dashed curve (labeled without excitons) corresponds to Fabry-Perot reflection. Inset: reflection spectrum for $n = 5, 6, 7$ exciton.

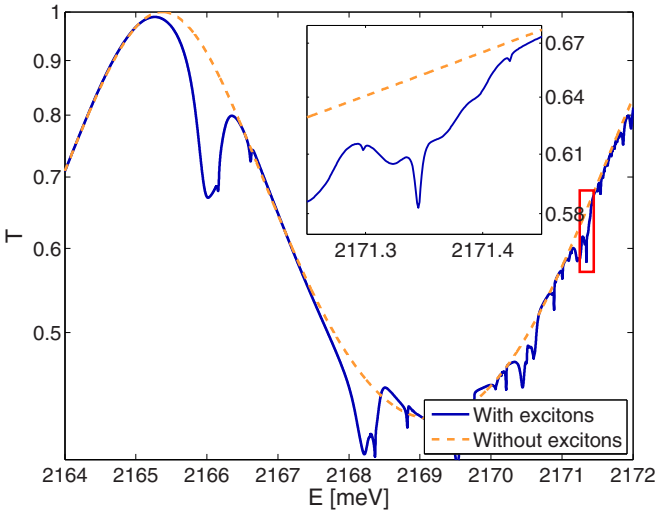

FIG. 9. The transmissivity coefficient of Cu_2O crystal of thickness 30 μm, when the magnetic field 2 T is applied. The dashed curve (labeled without excitons) corresponds to Fabry-Perot transmissivity. Inset: transmission spectrum for $n = 7$ exciton.

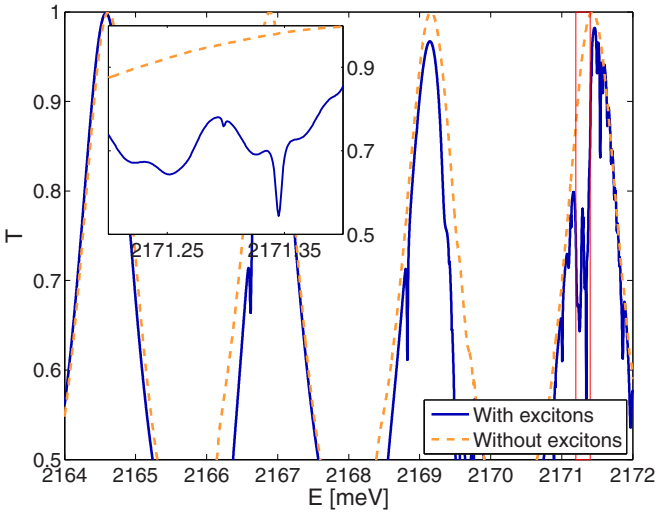

FIG. 11. The same as in Fig. 9, for crystal thickness 100 μm. Inset: transmission spectrum for $n = 7$ exciton.

see Eq. (41). The COM quantization approximation, used in our calculations, allowed us to calculate the reflection and transmission spectra, taking into account both the microscopic electronic excitations (excitons) and their interaction with the radiation field, resulting in creation of polariton modes. Having analytical formula for the reflection coefficient R and transmissivity T we are able to examine their dependence of the crystal size (Figs. 8–11). The calculations have been performed up to $N = 350$ and for excitonic states with principal number $n = 5$–7. One can observe the Fabry-Perot modes, typical for dielectric slab, with overlapping excitonic resonances. The Fabry-Perot resonance is dominant and strongly affects the reflection and transmission over the whole energy range and establishes the background on which the excitonic resonances

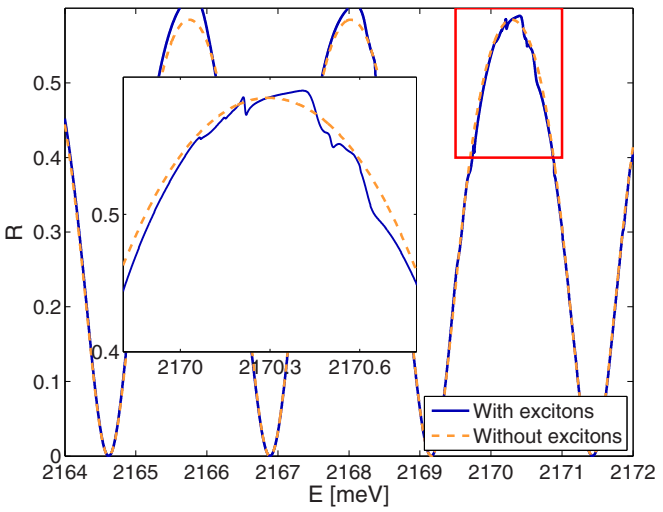

FIG. 10. The same as in Fig. 8, for crystal thickness 100 μm. Inset: reflection spectrum for $n = 7$ exciton.

appear, although the variations of R and T due to them have comparably smaller amplitudes. As can be seen from Figs. 8–11 the Fabry-Perot pattern strongly depends on the crystal size, which is consistent with Eqs. (33) and (34). In Figs. 8 and 9 magnetoreflectivity and magnetotransmissivity are presented for a sample of 30 μm and in such a case only one Fabry-Perot maximum is visible. For a thicker crystal of 100 μm the Fabry-Perot effect is more pronounced and more maxima appear (Figs. 10 and 11). The excitonic resonances approach each other and amplitudes of their changes are more distinct. All insets in Figs. 8–11 indicate that these two effects are readily separable.

VI. CONCLUSIONS

The main results of our paper can be summarized as follows. We have proposed a procedure based on the RDMA approach that allows us to obtain analytical expressions for the magneto-optical functions of semiconductor crystals including high number Rydberg excitons. Our results have general character because arbitrary exciton angular momentum number and arbitrary applied field strength are included. We have chosen the example of cuprous oxide, inspired by the recent experiment by Aßmann *et al.* [31]. We have calculated the magneto-optical functions (susceptibility, absorption, reflection, and transmission), obtaining a fairly good agreement between the calculated and the experimentally observed spectra. As each method using the iterative procedure, the present approach is a kind of approximation. Although we have solved the problem of excitons in a semiconductor when an external magnetic field is applied, we do not include the interaction between states with different n into the Hamiltonian we have used. It should be emphasized that the present approach is analytical until the last step in which the numerical code is used. The choice of dipole density model and therefore the oscillator strengths, which is an intricate function of free parameters, has an impact on the accuracy of our calculations and might be the source of discrepancy between theoretical and experimental results. Our results confirm the fundamental peculiarity of

magneto-optical effects: shifting, splitting, and, as a result for higher excitonic states, mixing of spectral lines. In particular, we obtained the splitting of P and F excitons, with increasing number of peaks corresponding to the increasing state number. All these interesting features of excitons with high n number which are examined and discussed on the basis of our theory might possibly provide deep insight into the nature of Rydberg excitons in solids and provoke their application to design all-optical flexible switches and future implementation in quantum information processing.

APPENDIX A: EXPANSION COEFFICIENTS $c_{Nn\ell m}$

Using the eigenfunctions (12) and transition dipole densities (22) and (23) we calculate the expansion coefficients $c_{Nn\ell m}$. For $n = 2,3$ we only have the coefficients related to the P excitons:

$$W_{N_1n1\pm1}c_{N_1n1\pm1} + V^{(n)}_{11\pm1}c_{N_1n1\pm1} = \langle w_{N_1}|E_x\rangle\langle R_{211}Y_{1\pm1}|M^{(1)}_x\rangle,$$
$$c_{N_1n1\pm1} = \frac{\langle w_{N_1}|E_x\rangle\langle R_{n11}Y_{1\pm1}|M^{(1)}_x\rangle}{W_{N_1n1\pm1} + V^{(n)}_{11\pm1}}. \tag{A1}$$

For $n \geqslant 4$ we must consider contributions of both excitons P and F. For $n = 4$ we have three equations,

$$\begin{aligned}
&W_{N_141\pm1}c_{N_141\pm1} + V^{(4)}_{11\pm1}c_{N_141\pm1} + V^{(4)}_{13\pm1}c_{N_143\pm1}\\
&\quad= \langle w_{N_1}|E_x\rangle\langle R_{411}Y_{1\pm1}|M^{(1)}_x\rangle,\\
&W_{N_143\pm1}c_{N_143\pm1} + V^{(4)}_{33\pm1}c_{N_143\pm1} + V^{(4)}_{31\pm1}c_{N_141\pm1}\\
&\quad= \langle w_{N_1}|E_x\rangle\langle R_{431}Y_{3\pm1}|M^{(3)}_x\rangle,\\
&W_{N_143\pm3}c_{N_143\pm3} + V^{(4)}_{33\pm3}c_{N_143\pm3} = \langle w_{N_1}|E_x\rangle\langle R_{433}Y_{3\pm3}|M^{(3)}_x\rangle,
\end{aligned} \tag{A2}$$

with solutions

$$\begin{aligned}
&c_{N_141\pm1}\\
&\quad= \langle w_{N_1}|E_x\rangle\frac{a_{22}\langle R_{411}Y_{1\pm1}|M^{(1)}_x\rangle - a_{12}\langle R_{431}Y_{3\pm1}|M^{(3)}_x\rangle}{\Delta},\\
&c_{N_143\pm1}\\
&\quad= \langle w_{N_1}|E_x\rangle\frac{a_{11}\langle R_{431}Y_{3\pm1}|M^{(3)}_x\rangle - a_{12}\langle R_{411}Y_{1\pm1}|M^{(1)}_x\rangle}{\Delta},\\
&c_{N_143\pm3} = \frac{\langle w_{N_1}|E_x\rangle\langle R_{433}Y_{3\pm3}|M^{(3)}_x\rangle}{W_{N_143\pm3} + V^{(4)}_{33\pm3}},\\
&\Delta = a_{11}a_{22} - a_{12}^2,\\
&a_{11} = W_{N_141\pm1} + V^{(4)}_{11\pm1}, \quad a_{12} = V^{(4)}_{13\pm1} = a_{21},\\
&a_{22} = W_{N_143\pm1} + V^{(4)}_{33\pm1}.
\end{aligned} \tag{A3}$$

In a similar way, the higher-order coefficients can be determined:

$$\begin{aligned}
&c_{N_1n3\pm3} = \frac{\langle w_{N_1}|E_x\rangle\langle R_{n33}Y_{3\pm3}|M^{(3)}_x\rangle}{W_{N_1n3\pm3} + V^{(n)}_{33\pm3}},\\
&c_{N_1n1\pm1}\\
&\quad= \langle w_{N_1}|E_x\rangle\frac{a_{22}\langle R_{n11}Y_{1\pm1}|M^{(1)}_x\rangle - a_{12}\langle R_{n31}Y_{3\pm1}|M^{(3)}_x\rangle}{a_{11}a_{22} - a_{12}^2},\\
&c_{N_1n3\pm1}\\
&\quad= \langle w_{N_1}|E_x\rangle\frac{a_{11}\langle R_{n31}Y_{3\pm1}|M^{(3)}_x\rangle - a_{12}\langle R_{n11}Y_{1\pm1}|M^{(1)}_x\rangle}{a_{11}a_{22} - a_{12}^2},\\
&a_{11} = W_{N_1n1\pm1} + V^{(n)}_{11\pm1}, \quad a_{12} = V^{(n)}_{13\pm1} = a_{21},\\
&a_{22} = W_{N_1n3\pm1} + V^{(n)}_{33\pm1}, \quad \Delta = a_{11}a_{22} - a_{12}^2,\\
&c_{N_1n1\pm1}\\
&\quad= \pm\frac{\langle w_{N_1}|E_x\rangle\left(\frac{r_0}{a^*}\right)\sqrt{\frac{2}{3}\pi}\,M_{10}\frac{1}{a^{*3/2}}\sqrt{\frac{n^2-1}{n^5}}}{\left(W_{N_1n1\pm1} + V^{(n)}_{111}\right)\left(W_{N_1n3\pm1} + V^{(n)}_{331}\right) - \left(V^{(n)}_{131}\right)^2}\\
&\qquad\times\left\{i\eta_{11}^{5/2}\left(W_{N_1n3\pm1} + V^{(n)}_{331}\right)\right.\\
&\qquad\left.+\,0.015\,272V^{(n)}_{131}\left(\frac{r_0}{a^*}\right)^2\eta_{31}^{9/2}\sqrt{\frac{(n^2-9)(n^2-4)}{n^4}}\right\},\\
&c_{N_1n3\pm1}\\
&\quad= \mp\frac{\langle w_{N_1}|E_x\rangle\left(\frac{r_0}{a^*}\right)\sqrt{\frac{2}{3}\pi}\,M_{10}\frac{1}{a^{*3/2}}\sqrt{\frac{n^2-1}{n^5}}}{\left(W_{N_1n1\pm1} + V^{(n)}_{111}\right)\left(W_{N_1n3\pm1} + V^{(n)}_{331}\right) - \left(V^{(n)}_{131}\right)^2}\\
&\qquad\times\left\{\left[W_{N_1n1\pm1} + V^{(n)}_{111}\right]0.015\,272\left(\frac{r_0}{a^*}\right)^2\eta_{31}^{9/2}\right.\\
&\qquad\left.\times\sqrt{\frac{(n^2-9)(n^2-4)}{n^4}} + V^{(n)}_{131}i\eta_{11}^{5/2}\right\}.
\end{aligned} \tag{A4}$$

APPENDIX B: DETERMINATION OF THE QUANTITIES $\langle R_{n11}Y_{1\pm1}|M^{(1)}_x\rangle, \langle R_{n31}Y_{3\pm1}|M^{(3)}_x\rangle, \langle R_{n33}Y_{3\pm3}|M^{(3)}_x\rangle$

Below we calculate the quantities $\langle R_{n11}Y_{1\pm1}|M^{(1)}_x\rangle$, $\langle R_{n31}Y_{3\pm1}|M^{(3)}_x\rangle, \langle R_{n33}Y_{3\pm3}|M^{(3)}_x\rangle$, which enter in the above derived formulas for the coefficients $c_{Nn\ell m}$. Using the definition (22) and (23) one obtains

$$\begin{aligned}
&\langle R_{n11}Y_{1\pm1}|M^{(1)}_x x\rangle\\
&\quad= \mp\sqrt{\frac{8\pi}{3}}\frac{M_{10}}{4ir_0^2}\int_0^\infty r^2dr\;\frac{r + r_0}{r^2}e^{-r/r_0}R_{n11}(r).
\end{aligned} \tag{B1}$$

Inserting on the right-hand side the expression for the radial function R_{n11} [see Eq. (12)] we get

$$\begin{aligned}\left\langle R_{n11}Y_{1\pm1}\middle|M_x^{(1)}x\right\rangle &= \mp\sqrt{\frac{8\pi}{3}}\frac{M_{10}}{4ir_0^2}\int_0^\infty dr\ (r+r_0)e^{-\lambda r}\left(\frac{2\eta_{11}}{na^*}\right)^{3/2}\frac{1}{3!}\\ &\times\sqrt{\frac{(n+1)!}{2n(n-2)!}}\left(\frac{2\eta_{11}r}{na^*}\right)M\left(-n+2,4,\frac{2\eta_{11}r}{na^*}\right), \quad \text{(B2)}\end{aligned}$$

where $\lambda=\frac{1}{r_0}+\frac{\eta_{11}}{na^*}=\frac{na^*+\eta_{11}r_0}{na^*r_0}$. The right-hand side of Eq. (B2) consists of two parts:

$$\begin{aligned}I_1 &= \sqrt{\frac{8\pi}{3}}\frac{M_{10}}{4ir_0^2}\left(\frac{2\eta_{11}}{na^*}\right)^{3/2}\left(\frac{2\eta_{11}}{na^*}\right)\\ &\times\frac{1}{3!}\sqrt{\frac{(n+1)!}{2n(n-2)!}}\int_0^\infty dr\ r^2\,e^{-\lambda r}M\left(-n+2,4,\frac{2\eta_{11}r}{na^*}\right)\\ &= \sqrt{\frac{8\pi}{3}}\frac{M_{10}}{4ir_0^2}\left(\frac{2\eta_{11}}{na^*}\right)^{5/2}\frac{1}{3!}\sqrt{\frac{(n+1)!}{2n(n-2)!}}\Gamma(3)\lambda^{-3}\\ &\times F\left(-n+2,3,4,\frac{2\eta_{11}r_0}{na^*+\eta_{11}r_0}\right), \quad \text{(B3)}\\ I_2 &= \sqrt{\frac{8\pi}{3}}\frac{M_{10}}{4ir_0^2}r_0\left(\frac{2\eta_{11}}{na^*}^{5/2}\right)\frac{1}{3!}\sqrt{\frac{(n+1)!}{2n(n-2)!}}\\ &\times\int_0^\infty rdr\ e^{-\lambda r}M\left(-n+2,4,\frac{2\eta_{11}}{na^*}r\right)\\ &= \sqrt{\frac{8\pi}{3}}\frac{M_{10}}{4ir_0^2}r_0\lambda^{-2}\left(\frac{2\eta_{11}}{na^*}\right)^{5/2}\frac{1}{3!}\sqrt{\frac{(n+1)!}{2n(n-2)!}}\\ &\times F\left(-n+2,2,4,\frac{2\eta_{11}r_0}{na^*+\eta_{11}r_0}\right), \quad \text{(B4)}\end{aligned}$$

$F(\alpha,\beta,\gamma,z)$ being the hypergeometric series. Performing the summation we obtain

$$I_1+I_2\approx\sqrt{\frac{8\pi}{3}}\frac{M_{10}r_0}{8i}\left(\frac{2\eta_{11}}{na^*}\right)^{5/2}\sqrt{\frac{(n+1)!}{2n(n-2)!}},$$

where the assumption $r_0<a^*$ has been used. Finally

$$\left\langle R_{n11}Y_{1\pm1}\middle|M_x^{(1)}\right\rangle=\mp\sqrt{\frac{2\pi(n^2-1)}{3n^5}}\frac{M_{10}}{\mathrm{i}}\left(\frac{r_0}{a^*}\right)\frac{\eta_{11}^{5/2}}{a^{*3/2}}. \quad \text{(B5)}$$

The following expression will be useful in calculation of oscillator strengths:

$$|I_1+I_2|^2=\frac{2}{3}\pi|M_{10}|^2\left(\frac{r_0}{a^*}\right)^2\frac{\eta_{11}^5}{a^{*3}}\frac{n^2-1}{n^5}. \quad \text{(B6)}$$

In the next step we calculate the quantity $\langle R_{n31}Y_{3\pm1}|M_x^{(3)}x\rangle$. Using the definitions (21) and (12) one obtains

$$\begin{aligned}\left\langle R_{n31}Y_{3\pm1}\middle|M_x^{(3)}x\right\rangle &= \mp\sqrt{\frac{3\pi}{7}}\frac{M_{10}}{r_0}\int_0^\infty dr\ e^{-r/r_0}R_{n31}(r)\\ &= \mp\sqrt{\frac{3\pi}{7}}\frac{M_{10}}{r_0}\left(\frac{2\eta_{31}}{na^*}\right)^{9/2}\int_0^\infty dr\ r^3\,e^{-\lambda r}\frac{1}{7!}\sqrt{\frac{(n+3)!}{2n(n-4)!}}\\ &\times M\left(-n+4,8,\frac{2\eta_{31}}{na^*}r\right)\end{aligned}$$

with

$$\lambda=\frac{1}{r_0}+\frac{\eta_{31}}{na^*}=\frac{na^*+\eta_{31}r_0}{na^*r_0}.$$

Performing the integration we arrive at the formulas

$$\begin{aligned}\left\langle R_{n31}Y_{3\pm1}\middle|M_x^{(3)}\right\rangle &= \mp\sqrt{\frac{3\pi}{7}}\frac{M_{10}}{r_0}\left(\frac{2\eta_{31}}{na^*}\right)^{9/2}\sqrt{\frac{(n+3)!}{2n(n-4)!}}\\ &\times\frac{3!}{7!}\lambda^{-4}\,F\left(-n+4,4,8,\frac{2\eta_{31}}{na^*\lambda}\right)\\ &\approx\mp\,0.015\,272\sqrt{\frac{2}{3}\pi}M_{10}\left(\frac{r_0}{a^*}\right)^3\frac{\eta_{31}^{9/2}}{a^{*3/2}}\\ &\times\sqrt{\frac{(n^2-9)(n^2-4)(n^2-1)}{n^9}},\end{aligned}$$

where again the assumption $r_0<a^*$ has been used. The formula

$$\begin{aligned}\left|\left\langle R_{n31}Y_{3\pm1}\middle|M_x^{(3)}\right\rangle\right|^2 &\approx 2.332\times10^{-4}\frac{2}{3}\pi\frac{|M_{10}|^2}{a^{*3}}(\eta_{31})^9\left(\frac{r_0}{a^*}\right)^6\\ &\times\frac{(n^2-9)(n^2-4)(n^2-1)}{n^9},\end{aligned}$$

will be used in calculations of the oscillator strengths related to the F exciton. The remaining formulas, connected to the $Y_{3,\pm3}$ harmonics, have the form

$$\begin{aligned}&\left\langle R_{n33}Y_{3\pm3}\middle|M_x^{(3)}\right\rangle\\ &= \mp\sqrt{\frac{5\pi}{7}}\frac{M_{10}}{r_0}\left(\frac{2\eta_{33}}{na^*}\right)^{9/2}\sqrt{\frac{(n+3)!}{2n(n-4)!}}\frac{3!}{7!}\lambda^{-4}\\ &\times F\left(-n+4,4,8,\frac{2\eta_{33}}{na^*\lambda}\right)\\ &\left|\left\langle R_{n33}Y_{3\pm3}\middle|M_x^{(3)}\right\rangle\right|^2\\ &\approx 3.887\times10^{-4}\frac{2}{3}\pi\frac{|M_{10}|^2}{a^{*3}}(\eta_{33})^9\left(\frac{r_0}{a^*}\right)^6\\ &\times\frac{(n^2-9)(n^2-4)(n^2-1)}{n^9}.\end{aligned}$$

APPENDIX C: DERIVATION OF THE MATRIX ELEMENTS $V_{\ell\ell_1mm_1}^{(nn_1)}$

In order to calculate the matrix elements $V_{\ell\ell_1mm_1}^{(nn_1)}$, as defined in Eq. (27), we start with the integral containing the angular dependence,

$$\begin{aligned}I_{\ell\ell_1mm_1} &= \left\langle Y_{\ell_1m_1}\middle|\sin^2\theta|Y_{\ell m}\right\rangle=\int d\Omega\ Y_{\ell_1m_1}^*(1-\cos^2\theta)Y_{\ell m}\\ &= \delta_{\ell\ell_1}\delta_{mm_1}-\int d\Omega\ Y_{\ell_1m_1}\cos^2\theta\,Y_{\ell m}. \quad \text{(C1)}\end{aligned}$$

Making use of the definition of the spherical harmonic functions,

$$Y_{\ell m}(\theta,\phi)=\sqrt{\frac{(2\ell+1)(\ell-m)!}{4\pi(\ell+m)!}}P_\ell^m(\cos\theta)e^{im\phi}, \tag{C2}$$

in terms of the associated Legendre polynomials P_ℓ^m, the second of the integrals on the right-hand side of Eq. (C1) can be put into the form

$$\begin{aligned} I &= \int d\Omega\, Y^*_{\ell_1 m_1}\cos^2\theta\, Y_{\ell m} \\ &= \delta_{mm_1}2\pi\sqrt{\frac{(2\ell+1)(\ell-m)!}{4\pi(\ell+m)!}\frac{(2\ell_1+1)(\ell_1-m_1)!}{4\pi(\ell_1+m_1)!}} \\ &\quad\times\int_{-1}^{+1}dx\, P_\ell^m(x)x^2P_{\ell_1}^{m_1}(x). \end{aligned} \tag{C3}$$

Making use of the recurrence relation for Legendre polynomials [57] we arrive at the integral

$$\begin{aligned} &\int_{-1}^{+1}dx\, P_\ell^m(x)x^2P_{\ell_1}^{m_1}(x) \\ &= \int_{-1}^{+1}dx\left\{\frac{1}{2\ell+1}\left[(\ell-m+1)P_{\ell+1}^m(x)+(\ell+m)P_{\ell-1}^m(x)\right]\right. \\ &\quad\left.\times\frac{1}{2\ell_1+1}\left[(\ell_1-m+1)P_{\ell_1+1}^m(x)+(\ell_1+m)P_{\ell_1-1}^m(x)\right]\right\}. \end{aligned} \tag{C4}$$

Performing the multiplication and integration, using the orthogonality relation for Legendre polynomials one obtains

$$\begin{aligned} &\int_{-1}^{+1}dx\, P_\ell^m(x)x^2P_{\ell_1}^{m_1}(x) \\ &= \frac{2(2\ell^2+2\ell-1-2m^2)(\ell+m)!}{(2\ell-1)(2\ell+1)(2\ell+3)(\ell-m)!}\delta_{\ell\ell_1} \\ &\quad+\frac{2(\ell-m+1)(\ell+m+2)(\ell+m+1)!}{(2\ell+1)(2\ell+3)(2\ell+5)(\ell+1-m)!}\delta_{\ell+1,\ell_1-1} \\ &\quad+\frac{2(\ell-m-1)(\ell+m)(\ell+m-1)!}{(2\ell-3)(2\ell-1)(2\ell+1)(\ell-1-m)!}\delta_{\ell_1+1,\ell-1}. \end{aligned} \tag{C5}$$

Inserting the above result into Eq. (C3) gives for the angular integration

$$\begin{aligned} I &= \delta_{mm_1}2\pi\sqrt{\frac{(2\ell+1)(\ell-m)!}{4\pi(\ell+m)!}\frac{(2\ell_1+1)(\ell_1-m_1)!}{4\pi(\ell_1+m_1)!}} \\ &\quad\times\left[\frac{2(2\ell^2+2\ell-1-2m^2)(\ell+m)!}{(2\ell-1)(2\ell+1)(2\ell+3)(\ell-m)!}\delta_{\ell\ell_1}\right. \\ &\quad+\frac{2(\ell-m+1)(\ell+m+2)(\ell+m+1)!}{(2\ell+1)(2\ell+3)(2\ell+5)(\ell+1-m)!}\delta_{\ell+1,\ell_1-1} \\ &\quad\left.+\frac{2(\ell-m-1)(\ell+m)(\ell+m-1)!}{(2\ell-3)(2\ell-1)(2\ell+1)(\ell-1-m)!}\delta_{\ell_1+1,\ell-1}\right]. \end{aligned} \tag{C6}$$

Using the above results we obtain the diagonal matrix element $V^{nn_1}_{\ell\ell_1 mm_1}$ when $n=n_1$,

$$\begin{aligned} &V^n_{\ell_1\ell_1m_1m_1} \\ &= \frac{R^*}{4}\gamma^2\delta_{\ell\ell_1mm_1}\left(1-\frac{2\ell_1^2+2\ell_1-1-2m_1^2}{(2\ell_1-1)(2\ell_1+3)}\right) \\ &\quad\times\int_0^\infty d\rho\rho^4\, R_{n\ell}R_{n_1\ell_1} \\ &= \delta_{\ell\ell_1mm_1}\frac{R^*}{4}\gamma^2\frac{2(\ell^2+\ell+m^2-1)}{(2\ell-1)(2\ell+3)}\int_0^\infty d\rho\,\rho^4\,[R_{n\ell}(\rho)]^2 \\ &= \delta_{\ell\ell_1mm_1}\frac{R^*}{4}\gamma^2\frac{(\ell^2+\ell+m^2-1)}{(2\ell-1)(2\ell+3)}\left(\frac{n}{\eta_{\ell m}}\right)^2 \\ &\quad\times[5n^2+1-3\ell(\ell+1)], \end{aligned} \tag{C7}$$

where we used the formula (for example [58] where $\eta_{\ell m}=1$)

$$\langle\rho^2\rangle=\tfrac{1}{2}[5n^2+1-3\ell(\ell+1)]. \tag{C8}$$

In a similar way the off-diagonal elements can be computed with the results displayed in Eq. (26). The integrals containing the radial eigenfunctions $R_{n\ell m}$, by using the relation between the hypergeometric function and the Laguerre polynomials, can be expressed by the integrals

$$\begin{aligned} I_{n\ell sm} &= \int_0^\infty d\rho\rho^4\, R_{n\ell m}R_{nsm} \\ &= \left(\frac{n}{2\eta_{\ell m}}\right)^2\sqrt{\frac{(n-\ell-1)!}{2n(n+\ell)!}}\sqrt{\frac{(n-s-1)!}{2n(n+s)!}} \\ &\quad\times\int_0^\infty x^{\ell+s+4}L^{2\ell+1}_{n-\ell-1}(x)L^{2s+1}_{n-s-1}(x)e^{-x}dx. \end{aligned}$$

For example, taking $n=4,\ell=1,s=3,m=1$, one has

$$\begin{aligned} I_{4131} &= \int_0^\infty d\rho\rho^4\, R_{411}R_{431} \\ &= \left(\frac{1}{\eta_{10}}\right)^2 8!\sqrt{\frac{1}{5!8!}}(90-90+20) \\ &= 20\left(\frac{1}{\eta_{10}}\right)^2\sqrt{\frac{8!}{5!}}\approx 367\left(\frac{1}{\eta_{10}}\right)^2. \end{aligned}$$

APPENDIX D: CALCULATION OF THE COEFFICIENTS $\langle w_N|E\rangle$

The homogeneous solution of the field equation (18) can be put into the form

$$E_{\rm hom}(Z)=Ae^{ik_bZ}+Be^{-ik_bZ}, \tag{D1}$$

where

$$\begin{aligned} A &= \frac{2k_0}{(k_0+k_b)W}e^{-ik_bL}E_{\rm in}, \\ B &= \frac{2k_0(k_b-k_0)}{(k_0+k_b)^2W}e^{ik_bL}E_{\rm in}. \end{aligned} \tag{D2}$$

With these expressions one obtains for $\langle w_N|E\rangle$

$$\langle w_N|E\rangle = AI+BI^*, \tag{D3}$$

with the notation

$$I = \langle w_N | \, e^{\mathrm{i}k_b Z} \rangle = \sqrt{\frac{2}{L}} \int_0^L \sin \frac{N\pi}{L} Z \, e^{\mathrm{i}k_b Z} dZ. \tag{D4}$$

With the use of the relations

$$\sin x = \frac{e^{\mathrm{i}x} - e^{-ix}}{2\mathrm{i}}, \quad e^{\pm iN\pi} = \cos N\pi, \tag{D5}$$

the integral I becomes

$$I = I_N = \sqrt{2L}(1 - \cos\, N\pi \exp[\mathrm{i}k_b L]) \frac{N\pi}{(N\pi)^2 - (k_b L)^2}. \tag{D6}$$

The quantity I_N^2/L which appears in the expressions for the optical functions, has the form

$$\frac{I_N^2}{L} = \frac{2N^2\pi^2}{[(k_b L)^2 - N^2\pi^2]^2}(1 - \cos\, N\pi \exp[\mathrm{i}k_b L])^2. \tag{D7}$$

The expression $k_b L$ can be transformed to $k_b L = \frac{\hbar\omega}{\hbar c}\sqrt{\epsilon_b} L = \frac{E}{E_L}$. For Cu_2O, $\epsilon_b = 7.5$, so $E_L = \frac{72.3}{L}$ meV; L is expressed in μm and for the probe of length $L = 30$ μm one gets $E_L = 2.41$ meV. Since $I_N = I_N^*$ one obtains

$$\langle w_N | E_{\mathrm{hom}}(Z) \rangle = I_N(A + B) = I_N E_{\mathrm{hom}}(0), \tag{D8}$$

where

$$E_{\mathrm{hom}}(0) = E_{\mathrm{in}} \frac{1 + r_\infty}{1 - r_\infty^2 \exp(i\Theta)}(1 - r_\infty e^{\mathrm{i}\Theta}). \tag{D9}$$

APPENDIX E: OPTICAL FUNCTIONS

Below we derive the formulas (33) and (34). They will be obtained from Eq. (16) by using the total electric field $E(Z) = E_{\mathrm{hom}}(Z) + E_{\mathrm{nhom}}(Z)$. In particular, for the reflection coefficient one obtains

$$R = |r|^2, \tag{E1}$$

with

$$r = r_0 + r_{\mathrm{exc}}, \quad r_0 = \frac{r_\infty(1 - e^{\mathrm{i}\Theta})}{1 - r_\infty^2 e^{\mathrm{i}\Theta}},$$

$$r_{\mathrm{exc}} = \frac{k_0^2}{\epsilon_0 E_{\mathrm{in}}} \int_0^L G^E(0,Z) P_{\mathrm{exc}}(Z) dZ. \tag{E2}$$

Since

$$G^E(0,Z) = \frac{i(1 - r_\infty)}{2k_b\big(1 - r_\infty^2 \, e^{\mathrm{i}\Theta}\big)}(e^{\mathrm{i}k_b Z} - r_\infty \, e^{\mathrm{i}\Theta - \mathrm{i}k_b Z}), \tag{E3}$$

we obtain

$$\begin{aligned} r_{\mathrm{exc}} &= \frac{k_0^2}{\epsilon_0 E_{\mathrm{in}}} \int_0^L G^E(0,Z) P_{\mathrm{eks}}(Z) dZ \\ &= \frac{k_0^2}{2\epsilon_0 E_{\mathrm{in}}} \frac{\mathrm{i}(1 - r_\infty)}{k_b\big(1 - r_\infty^2 \, e^{\mathrm{i}\Theta}\big)} \\ &\quad \times \sum_N [\langle w_N | e^{\mathrm{i}k_b Z} \rangle - r_\infty \, e^{\mathrm{i}\Theta} \langle w_N | e^{-\mathrm{i}k_b Z} \rangle] P_N \\ &= \frac{k_0^2}{2\epsilon_0 E_{\mathrm{in}}} \frac{i(1 - r_\infty)}{k_b\big(1 - r_\infty^2 \, e^{\mathrm{i}\Theta}\big)}(1 - r_\infty \, e^{\mathrm{i}\Theta}) \sum_N I_N P_N, \end{aligned}$$

from which, with respect to Eq. (28), we get

$$\begin{aligned} r_{\mathrm{exc}} &= \frac{k_0^2 E_{\mathrm{hom}}(0)}{2E_{\mathrm{in}}} \frac{\mathrm{i}(1 - r_\infty)}{k_b\big(1 - r_\infty^2 \, e^{\mathrm{i}\Theta}\big)}(1 - r_\infty \, e^{\mathrm{i}\Theta}) \\ &\quad \times \epsilon_b \sum_N I_N^2 \sum_{n\ell m} \Delta_{LT}^{(P)} \chi_{Nn\ell m}. \end{aligned} \tag{E4}$$

Inserting in the above equation the expression (D9), we obtain

$$\begin{aligned} r_{\mathrm{exc}} &= \frac{\mathrm{i}}{2} \frac{(k_b L)\big(1 - r_\infty^2\big)}{\big(1 - r_\infty^2 \, e^{\mathrm{i}\Theta}\big)^2}(1 - r_\infty \, e^{\mathrm{i}\Theta})^2 \\ &\quad \times \sum_N \left(\frac{I_N^2}{L}\right) \sum_{n\ell m} \Delta_{LT}^{(P)} \chi_{Nn\ell m}. \end{aligned} \tag{E5}$$

Now the total complex reflection coefficient r has the following form:

$$\begin{aligned} r &= r_0 + r_{\mathrm{exc}} \\ &= r_0 \Bigg[1 + \mathrm{i}\left(\frac{E}{2E_L}\right) \frac{\big(1 - r_\infty^2\big)(1 - r_\infty e^{\mathrm{i}\Theta})^2\big(1 - r_\infty^2 e^{\mathrm{i}\Theta}\big)}{r_\infty(1 - e^{\mathrm{i}\Theta})} \\ &\quad \times \sum_N \left(\frac{I_N^2}{L}\right) \sum_{n\ell m} \Delta_{LT}^{(P)} \chi_{Nn\ell m} \Bigg], \end{aligned} \tag{E6}$$

which, using Eq. (E1) immediately gives the result (33). Analogically, we determine the transmissivity

$$T = \left| \frac{E(L)}{E_{\mathrm{in}}} \right|^2, \tag{E7}$$

resulting from the equation

$$T = |t|^2, \tag{E8}$$

where

$$t = t_0 + t_{\mathrm{exc}}, \quad t_0 = \frac{1 - r_\infty^2}{1 - r_\infty^2 e^{\mathrm{i}\Theta}} e^{\mathrm{i}\Theta/2},$$

$$t_{\mathrm{exc}} = \frac{k_0^2}{\epsilon_0 E_{\mathrm{in}}} \int_0^L G^E(L,Z) P_{\mathrm{exc}}(Z) dZ. \tag{E9}$$

Since

$$G^E(L,Z) = \frac{\mathrm{i}e^{\mathrm{i}\Theta/2}(1 - r_\infty)}{2k_b\big(1 - r_\infty^2 e^{\mathrm{i}\Theta}\big)}(e^{-ik_b Z} - r_\infty e^{ik_b Z}),$$

we have

$$\begin{aligned} t_{\mathrm{exc}} &= \frac{k_0^2}{E_{\mathrm{in}}} \int_0^L G^E(L,Z) P_{\mathrm{exc}}(Z) dZ \\ &= \frac{(k_b L)}{2} \frac{\mathrm{i}e^{\mathrm{i}\Theta/2}(1 - r_\infty)}{\big(1 - r_\infty^2 e^{\mathrm{i}\Theta}\big)^2}(1 + r_\infty)(1 - r_\infty \, e^{\mathrm{i}\Theta}) \\ &\quad \times \sum_N \left(\frac{I_N^2}{L}\right) \sum_{n\ell m} \Delta_{LT}^{(P)} \chi_{Nn\ell m}, \end{aligned}$$

and

$$\begin{aligned} t = t_0 + t_{\mathrm{exc}} = t_0 \Bigg[1 + \mathrm{i}\left(\frac{E}{2E_L}\right) \frac{(1 - r_\infty e^{\mathrm{i}\Theta})}{\big(1 - r_\infty^2 e^{\mathrm{i}\Theta}\big)} \\ \times \sum_N \left(\frac{I_N^2}{L}\right) \sum_{n\ell m} \Delta_{LT}^{(P)} \chi_{Nn\ell m} \Bigg]. \end{aligned} \tag{E10}$$

Inserting the above result into Eq. (E8), we obtain the transmissivity (34).

APPENDIX F: DERIVATION OF THE QUANTITIES $\chi_{Nn\ell m}$

Using the dispersion relation

$$\frac{c^2k^2}{\omega^2} = \epsilon_b + \frac{2}{\epsilon_0}\int d^3r M^* Y,$$

$$\frac{2}{\epsilon_0}\int d^3r M^* Y = \frac{2}{\epsilon_0}\int d^3r M_x^{(1)*}\sum_{n\ell m} c_{Nn\ell m} R_{n\ell m} Y_{\ell m} + \frac{2}{\epsilon_0}\int d^3r M_x^{(3)*}\sum_{n\ell m} c_{Nn\ell m} R_{n\ell m} Y_{\ell m} \quad \text{(F1)}$$

we define the quantities $\chi_{Nn\ell m}$ and $\tilde{\chi}_{Nn\ell m}$:

$$\frac{2}{\epsilon_0}\int d^3r M_x^{(1)*} c_{N_1 n1\pm1} R_{n11} Y_{1\pm1} = \epsilon_b \Delta_{LT}^{(P)} \tilde{\chi}_{N_1 n1\pm1} \langle E_x | w_{N_1}\rangle,$$
$$\frac{2}{\epsilon_0}\int d^3r M_x^{(3)*} c_{N_1 n3\pm1} R_{n31} Y_{3\pm1} = \epsilon_b \Delta_{LT}^{(P)} \tilde{\chi}_{N_1 n3\pm1} \langle E_x | w_{N_1}\rangle,$$
$$\frac{2}{\epsilon_0}\int d^3r M_x^{(3)*} c_{N_1 n3\pm3} R_{n33} Y_{3\pm3} = \epsilon_b \Delta_{LT}^{(P)} \tilde{\chi}_{N_1 n3\pm3} \langle E_x | w_{N_1}\rangle. \quad \text{(F2)}$$

The notation $\tilde{\chi}$ denotes that the formula contains contributions from both excitons P and F. Using the formulas (22) and (23), and the expressions $\langle R_{n11} Y_{1\pm1} | M_x^{(1)}\rangle, \langle R_{n31} Y_{3\pm1} | M_x^{(3)}\rangle$, $\langle R_{n33} Y_{3\pm3} | M_x^{(3)}\rangle$ derived in Appendix B, we obtain obtaining the following formulas: for $n = 2,3$

$$\chi_{Nn1\pm1} = \frac{f_{n11}}{W_{n1\pm1} + V_{11\pm1}^{(n)}}, \quad f_{n11} = \frac{16}{3}\frac{n^2-1}{n^5}. \quad \text{(F3)}$$

For $n \geqslant 4$ we observe the overlapping of the P and F excitons, which is reflected in the formulas

$$\chi_{Nn3\pm3} = \frac{f_{n33}}{W_{Nn3\pm3} + V_{33\pm3}^{(n)}},$$
$$f_{n33} = 2.073\times10^{-3}\,\frac{\eta_{33}^9}{\eta_{11}^5}\left(\frac{r_0}{a^*}\right)^4 \frac{(n^2-9)(n^2-4)(n^2-1)}{n^9},$$
$$\tilde{\chi}_{Nn1\pm1} = \frac{f_{n11}\left\{\left(W_{Nn3\pm1} + V_{331}^{(n)}\right) - \mathrm{i}p_n V_{131}^{(n)}\right\}}{\left(W_{Nn1\pm1} + V_{111}^{(n)}\right)\left(W_{Nn3\pm1} + V_{331}^{(n)}\right) - \left(V_{131}^{(n)}\right)^2}, \quad \text{(F4)}$$

$$\tilde{\chi}_{N_1 n3\pm1} = \frac{f_{n11} p_n\left\{\left[W_{N_1 n1\pm1} + V_{111}^{(n)}\right]p_n + i\,V_{131}^{(n)}\right\}}{\left(W_{N_1 n1\pm1} + V_{111}^{(n)}\right)\left(W_{N_1 n3\pm1} + V_{331}^{(n)}\right) - \left(V_{131}^{(n)}\right)^2}$$
$$p_n = 0.015\,272\left(\frac{r_0}{a^*}\right)^2 \frac{\eta_{31}^{9/2}}{\eta_{11}^{5/2}}\sqrt{\frac{(n^2-9)(n^2-4)}{n^4}}. \quad \text{(F5)}$$

[1] Ya. J. Frenkel, Phys. Rev. **37**, 17 (1931); **37**, 1276 (1931).
[2] G. H. Wannier, Phys. Rev. **52**, 191 (1937).
[3] N. F. Mott, Trans. Faraday Soc. **34**, 500 (1938).
[4] E. F. Gross and N. A. Karriiev, Dokl. Akad. Nauk SSSR **84**, 471 (1952).
[5] R. S. Knox, *Theory of Excitons* (Academic, New York, 1963).
[6] V. M. Agranovich and V. L. Ginzburg, *Crystal Optics with Spatial Dispersion and Excitons* (Springer-Verlag, Berlin, 1984).
[7] A. Stahl and I. Balslev, *Electrodynamics of the Semiconductor Band Edge* (Springer-Verlag, Berlin, 1987).
[8] G. La Rocca, in *Electronic Excitations in Organic Based Nanostructures*, Thin Films and Nanostructures Vol. 31, edited by V. M. Agranovich and G. F. Bassani (Elsevier, Amsterdam, 2003), pp. 97–128.
[9] G. Czajkowski, F. Bassani, and L. Silvestri, Riv. Nuovo Cimento **26**, 1 (2003).
[10] V. M. Agranovich, *Excitations in Organic Solids* (Oxford University Press, Oxford, 2009).
[11] C. Weisbuch and B. Vinter, *Quantum Semiconductor Structures: Fundamentals and Applications* (Academic, New York, 1991).
[12] L. Banyai and S. W. Koch, *Semiconductor Quantum Dots* (World Scientific, Singapore, 1993).
[13] E. L. Ivchenko and G. E. Pikus, *Superlattices and Other Heterostructures. Symmetry and Optical Phenomena* (Springer-Verlag, Berlin, 1995).
[14] L. Woggon, *Optical Properties of Semiconductor Quantum Dots* (Springer-Verlag, Berlin, 1997).
[15] L. Jacak, P. Hawrylak, and A. Wojs, *Quantum Dots* (Springer-Verlag, Berlin, 1998).
[16] D. Bimberg, M. Grundmann, and N. N. Ledentsov, *Quantum Dot Heterostructures* (Wiley, New York, 1998).
[17] T. Chakraborty, *Quantum Dots* (Elsevier, Amsterdam, 1999).
[18] V. M. Ustinov, A. E. Zhukov, A. Yu. Egorov, and N. A. Maleev, *Quantum Dot Lasers* (Oxford University Press, Oxford, 2003).
[19] E. L. Wolf, *Nanophysics and Nanotechnology, An Introduction to Modern Concepts in Nanoscience* (Wiley, Weinheim, 2004).
[20] O. Manasreh, *Semiconductor Heterojunctions and Nanostructures* (McGraw-Hill, New York, 2005).
[21] P. Harrison, *Quantum Wells, Wires and Dots* (Wiley, New York, 2005).
[22] T. Kazimierczuk, D. Fröhlich, S. Scheel, H. Stolz, and M. Bayer, Nature (London) **514**, 343 (2014).
[23] S. Höfling and A. Kavokin, Nature (London) **514**, 313 (2014).
[24] J. Thewes, J. Heckötter, T. Kazimierczuk, M. Aßmann, D. Fröhlich, M. Bayer, M. A. Semina, and M. M. Glazov, Phys. Rev. Lett. **115**, 027402 (2015).
[25] J. Heckötter, Stark-effect measurements on Rydberg excitons in Cu_2O, Ph.D. thesis, Technical University Dortmund, 2015.
[26] S. Zielińska-Raczyńska, G. Czajkowski, and D. Ziemkiewicz, Phys. Rev. B **93**, 075206 (2016).
[27] F. Schweiner, J. Main, and G. Wunner, Phys. Rev. B **93**, 085203 (2016).
[28] F. Schöne, S.-O. Krüger, P. Grünwald, H. Stolz, S. Scheel, M. Aßmann, J. Heckötter, J. Thewes, D. Fröhlich, and M. Bayer, Phys. Rev. B **93**, 075203 (2016).

[29] M. Feldmaier, J. Main, F. Schweiner, H. Cartarius, and G. Wunner, J. Phys. B **49**, 144002 (2016).
[30] F. Schweiner, J. Main, G. Wunner, and C. Uihlein, Phys. Rev. B **94**, 115201 (2016).
[31] M. Aßmann, J. Thewes, D. Frölich, and M. Bayer, Nat. Mater. **15**, 741 (2016).
[32] S. Zielińska-Raczyńska, D. Ziemkiewicz, and G. Czajkowski, Phys. Rev. B **94**, 045205 (2016).
[33] F. Schweiner, J. Main, G. Wunner, M. Freitag, J. Heckötter, C. Uihlein, M. Aßmann, D. Fröhlich, and M. Bayer, Phys. Rev. B **95**, 035202 (2017).
[34] F. Schweiner, J. Main, and G. Wunner, Phys. Rev. Lett. **118**, 046401 (2017).
[35] S. Zielińska-Raczyńska, D. Ziemkiewicz, and G. Czajkowski, arXiv:1610.00131.
[36] J. Ningyuan, A. Georgakopoulos, A. Ryou, N. Schine, A. Sommer, and J. Simon, Phys. Rev. A **93**, 041802(R) (2016).
[37] H. Tuffigo, R. T. Cox, N. Magnea, Y. Merle d'Aubigné, and A. Million, Phys. Rev. B **37**, 4310(R) (1988).
[38] A. D'Andrea and R. Del Sole, Phys. Rev. B **41**, 1413 (1990).
[39] A. Tredicucci, Y. Chen, F. Bassani, J. Massies, C. Deparis, and G. Neu, Phys. Rev. B **47**, 10348 (1993).
[40] L. C. Andreani, in *Confined Electrons and Photons, New Physics and Applications*, edited by E. Burstein and C. Weisbuch (Plenum, New York, 1995), pp. 57–112.
[41] N. Tomassini, A. D'Andrea, R. Del Sole, H. Tuffigo-Ulmer, and R. T. Cox, Phys. Rev. B **51**, 5005 (1995).
[42] P. Lefebvre, V. Calvo, N. Magnea, J. Allègre, T. Taliercio, and H. Mathieu, J. Cryst. Growth **184-185**, 844 (1998).
[43] D. Dragoman and M. Dragoman, *Optical Characterization of Solids* (Springer, Berlin, 2002).
[44] J. J. Davies, D. Wolverson, V. P. Kochereshko, A. V. Platonov, R. T. Cox, J. Cibert, H. Mariette, C. Bodin, C. Gourgon, I. V. Ignatiev, E. V. Ubylvovk, Y. P. Efimov, and S. A. Eliseev, Phys. Rev. Lett. **97**, 187403 (2006).
[45] L. C. Smith, J. J. Davies, D. Wolverson, S. Crampin, R. T. Cox, J. Cibert, H. Mariette, V. P. Kochereshko, M. Wiater, G. Karczewski, and T. Wojtowicz, Phys. Rev. B **78**, 085204 (2008).
[46] V. P. Kochereshko, L. C. Smith, J. J. Davies, R. T. Cox, A. Platonov, D. Wolverson, H. Boukari, H. Mariette, J. Cibert, M. Wiater, T. Wojtowicz, and G. Karczewski, Phys. Status Solidi B **245**, 1059 (2008).
[47] *Strong Light-Matter Coupling. From Atoms to Solid-State Systems*, edited by A. Auffèves, D. Gerace, M. Richard, S. Portolan, M. de Franca Santos, L. Ch. Kwek, and Ch. Miniatura (World Scientific, Singapore, 2014).
[48] M. Abramowitz and I. Stegun, *Handbook of Mathematical Functions* (Dover, New York, 1965).
[49] G. Czajkowski, F. Bassani, and A. Tredicucci, Phys. Rev. B **54**, 2035 (1996).
[50] P. Schillak, Eur. Phys. J. B **84**, 17 (2011).
[51] P. Schillak and G. Czajkowski, Eur. Phys. J. B **88**, 253 (2015).
[52] C. F. Klingshirn, *Semiconductor Optics* (Springer, Heidelberg, 1995).
[53] F. Bassani, G. Czajkowski, and A. Tredicucci, Z. Phys. B **98**, 39 (1995).
[54] Ch. Uihlein, D. Fröhlich, and R. Kenklies, Phys. Rev B **23**, 2731 (1981).
[55] D. Fröhlich, A. Kulik, B. Uebbing, A. Mysyrowicz, V. Langer, H. Stolz, and W. von der Osten, Phys. Rev. Lett. **67**, 2343 (1991).
[56] J. Heckötter (private communication).
[57] I. S. Gradshteyn and I. M. Ryzhik, *Table of Integrals, Series, and Products* (Academic, San Diego, 1994).
[58] A. Messiah, *Quantum Mechanics* (North-Holland, Amsterdam, 1961).